Du J, Bao J, Lu C, Werner D.

Reductive sequestration of chromate by hierarchical FeS@Fe^0 particles.

***Water Research*, 2016**

DOI: http://dx.doi.org/10.1016/j.watres.2016.06.009

Reductive sequestration of chromate by hierarchical FeS@Fe^0 particles

Jiangkun Du [a], Jianguo Bao [*,a], Chenghang Lu [a], David Werner [b]

a. School of Environmental Studies, China University of Geosciences, Wuhan 430074, P. R. China

b. School of Civil Engineering and Geosciences, Newcastle University, Newcastle upon Tyne, NE1 7RU, England, U.K.

*Corresponding author:
Jianguo Bao
Email:bjianguo@cug.edu.cn
Tel. (+86)-27-67883470; Fax (+86)-27-87436235

Submitted to *Water Research*

As an original research

Abstract: Nanoscale Fe^0 can detoxify Cr(VI)-bearing wastewater and groundwater, but rapid passivation will be a negative factor for large-scale remediation applications. In this study, a magnetic FeS@Fe^0 hybrid material was fabricated by in situ immobilization of iron sulfide (FeS) onto Fe^0 particles to improve the Cr(VI) removal capacity. The solid characterization confirmed that Fe^0 particles were encapsulated by amorphous iron monosulfide. The Cr(VI) uptake by FeS@Fe^0 hybrid particles was found to follow pseudo-second-order rate kinetics, and the Langmuir isotherm was most suitable to describe the Cr(VI) sorption. Meanwhile, the FeS@Fe^0 hybrid particles showed much higher efficiencies towards Cr(VI) sequestration compared to individual nFe^0. Moreover, results of batch experiments with various adsorbent doses indicated that the reactivity of FeS@Fe^0 varies with different FeS-to-Fe^0 molar ratios. The reaction rate constants of Cr(VI) removal first increased with increasing FeS-to-Fe^0 ratio from 0/1 to 1/9, and then decreased for higher FeS-to-Fe^0 ratios of 1/5 or 1/3. For environmental parameters, there was a negative effect of increasing solution pH and dissolved oxygen on Cr(VI) removal. Furthermore, a mechanistic analysis revealed that the Cr(VI) reduction predominantly occurred at the solid-liquid interface, and that Fe(II) regenerated from FeS@Fe^0 corrosion may account for 52% of Cr(VI) reduction, while electrons from Fe^0 and FeS accounted for the rest. After the treatment, Cr(VI) became completely transformed and immobilized as solid Fe-Cr hydroxide precipitates, thus avoiding secondary contamination. The FeS@Fe^0 hybrid material shows improved potential for treating Cr(VI)-bearing wastewater compared to nano Fe^0.

***Keywords*:** Cr(VI); reduction; nanoscale zerovalent iron; FeS@Fe^0 hybrid particles

1. Introduction

Chromium (Cr), a prevalent metal contaminant, can be globally detected in industrial wastewater, surface water, groundwater and soils (Kamaludeen et al. 2003). Normally, Cr exists in oxidation states of Cr(III) and Cr(VI), which display contrasting toxicity and mobility (Dhal et al. 2013). Cr(III) has low toxicity and is recognized as an essential trace element for human nutrition. Cr(III) is easy to hydrolyze in aqueous solution, thus has a very low solubility and is inclined to attach on mineral surface. In contrast, Cr(VI) species, such as CrO_4^{2-} and $Cr_2O_7^{2-}$, are water soluble over a wide pH range. Cr(VI) is of serious concern due to its greater toxicity as compared to Cr(III), and Cr(VI) is a human carcinogen (Pettine et al. 1998, Cieślak-Golonka 1996). Unfortunately, Cr-bearing wastewaters produced from a wide range of industries, such as electroplating, ore mining, leather tanning, and pigment making, are dominated by anthropogenic Cr(VI) species (Dhal et al. 2013).

Nanoscale zerovalent iron (nFe^0) has attracted extensive interest for ex/in situ treatment of contaminants, such as chlorinated hydrocarbons and redox-sensitive heavy metals (Fu et al. 2014, Du et al. 2013, Huang et al. 2013). It has the advantages of large surface area, inexpensive cost, high reducibility, feasible in-situ operation and easy magnetic separation (Fu et al. 2014, Guan et al. 2015). Compared to other adsorbents, nFe^0 can transform highly soluble Cr(VI) to insoluble Cr(III) via coupled oxidation of Fe^0 and Fe(II), and subsequent formation of Cr(III)-Fe(III) precipitates (Manning et al. 2008, Ai et al. 2008, Hoch et al. 2008). After reactions, the Cr-laden iron could be magnetically separated avoiding secondary pollution risks. However, Fe^0 corrosion in aquatic media may negatively affect the Cr(III) detoxification process. Release of ferrous ions and formation of an oxide shell simultaneously occur during Fe^0 corrosion (Yoon et al. 2011). A thick surface oxide layer would significantly depress further Fe^0 corrosion and lead to material passivation (Melitas et al. 2001, Huang and Zhang 2005). Even though Cr(VI) could be directly reduced by surface electrons and Fe(II) produced via Fe^0 corrosion, fast Fe^0 passivation will result in a low rate of Cr(VI) reduction. Some multicomponent materials have been investigated to improve nFe^0 reactivity via accelerating electron transfer from the Fe^0 core (Kim et al. 2011, Fan et al. 2013, Lv et al. 2011). Mu et al. prepared a series of core-shell $Fe@Fe_2O_3$ nanowires for anoxic Cr(VI) removal (Mu et al. 2014). They found that a moderate thickness of the Fe_2O_3 shell

benefits the iron corrosion and electron transfer from the Fe^0 core. Lv et al. reported a synergistically enhanced removal of Cr(VI) by nFe^0-Fe_3O_4 nanocomposites due to a more facile electron transfer from nFe^0 to the Fe_3O_4 surface (Lv et al. 2011, Lv et al. 2014). These previous findings indicated that the hybrid materials with different components have advantages over single component materials.

Iron monosulfide (FeS) is a reactive mineral ubiquitous in anoxic soil and sediments. It was used as an effective remediation agent for removal of heavy metals and chlorinated hydrocarbons (Gong et al. 2014, Bi and Hayes 2014, Jeong and Hayes 2007). However, FeS alone is easily air-oxidized, thereby losing a considerable portion of its reductive activity. A mixed combination of nFe^0 and FeS might be a feasible way to exert a synergistic effect which is not available from the individual components. Very recently, Kim et al. reported a kind of S-doped nFe^0 (S-nFe^0) nanoparticles, which were prepared by adding sodium borohydride and dithionite mixture into ferric solutions to obtain a type of S-incorporated nFe^0 (Kim et al. 2014). Then Su et al. applied this kind of S-Fe^0 nanoparticles for adsorptive removal of cadmium (Cd) (Su et al. 2015). They found that the doping amount of dithionite played a crucial role in the reactivity of S-nFe^0 composite for Cd removal, and S-nFe^0 composite with a proper Fe/S ratio exhibited a larger adsorption capacity than pristine nFe^0. Compared to pristine nFe^0, preparation of these S-Fe^0 nanoparticles would produce large amounts of gaseous hydrogen sulfide (H_2S) generated from dithionite decomposition as shown in Eqs. (1~2) (Kim et al. 2011, Su et al. 2015). Simultaneously, FeS and Fe^0 is generated as a composite (Eqs (3-4)), which is composed of FeS and Fe^0 all over the particle body instead of pure Fe^0. However, according to their observations, vigorous H_2S was generated during S-Fe^0 synthesis, which should be a potential environmental concern. Instead, in situ synthesis of FeS in the presence of nFe^0 could realize a surface sulfidation of Fe^0 and avoid the generation of hydrogen sulfide (Fan et al. 2013).

$$2S_2O_4^{2-} + H_2O \rightarrow 2HSO_3^- + S_2O_3^{2-} \quad (1)$$

$$S_2O_4^{2-} + S_2O_3^{2-} + H^+ + 2H_2O \rightarrow H_2S\uparrow + 3HSO_3^- \quad (2)$$

$$Fe^{2+} + H_2S \rightarrow FeS\downarrow + 2H^+ \quad (3)$$

$$2Fe^{2+} + BH_4^- + 3H_2O \rightarrow 2Fe^0 + H_2BO_3^- + 4H^+ + 2H_2 \quad (4)$$

In the present study, new FeS@Fe^0 hybrid particles were fabricated via a two-step method.

First, nFe^0 was synthesized via chemical reduction by sodium borohydride. Then, FeS was successively synthesized in presence of nFe^0 by stoichiometric precipitation of Fe^{2+} and Na_2S, forming an encapsulated structure named as $FeS@Fe^0$. In addition, the formation of the $FeS@Fe^0$ hybrid material may also proceed naturally in the subsurface for reducing conditions via interaction between nFe^0 with abundant S^{2-}. The performance of this material on Cr(VI) removal was tested by comparison with pure nFe^0, and mechanisms are elucidated based on characterizations of SEM, XRD, FTIR, XPS, and experimental results. Magnetic properties of the composite particles can facilitate the separation of Cr-laden material at the end of treatments.

2. Materials and methods

2.1. Chemicals

Analytical grade chemicals were purchased from Sinopharm Chemical Reagent Co., Ltd. Cr(VI) stock solutions were synthesized by dissolving $K_2Cr_2O_7$. Solutions were prepared with deionized water, which was deoxygenated by bubbling N_2 gas through the solution for half an hour before use.

2.2. Preparation of nFe^0 and $FeS@Fe^0$ hybrid materials

$FeS@Fe^0$ hybrid particles were prepared via a two-step process (see Scheme S1 in supplementary material). First, nFe^0 was prepared by reduction with sodium borohydride. Briefly, 50 mL of $NaBH_4$ solution (0.8 mol/L) was added dropwise into 100 mL of $FeSO_4 \cdot 7H_2O$ (0.18 mol/L) solution under N_2 protection in a three-neck flask. Then, the black nFe^0 products were magnetically separated and rinsed with deoxygenated water three times to remove impurities. The overall process occurs according to Eq 5.

$$Fe^{2+} + 2BH_4^- + 6H_2O \rightarrow Fe^0 \downarrow + 2B(OH)_3 + 7H_2 \uparrow \quad (5)$$

For synthesis of $FeS@Fe^0$ hybrid particles, the above nFe^0 particles were immediately re-dispersed in 150 mL of $FeSO_4$ solution (the total amount of $FeSO_4$ was 0.002 mol). Subsequently, 50 mL of 0.04 mol/L Na_2S (the stoichiometric ratio of $Fe^{2+}{}_{mol}$: $S^{2-}{}_{mol}$ was equal to 1:1) was added dropwise into the flask to in situ generate $FeS@Fe^0$ hybrid particles as described by Eq. 6:

133 $Fe^{2+} + S^{2-} \rightarrow FeS\downarrow$ (6)

134 The hybrid particles were separated using an external magnet, thoroughly washed with
135 ethanol and deoxygenated water, and finally vacuum-dried at 60 °C overnight. The FeS@Fe^0
136 particles with different FeS contents were synthesized by changing the FeS_{mol} : Fe^0_{mol} ratio. In
137 the present research, four types of FeS@Fe^0 hybrid particles (FeS_{mol} : Fe^0_{mol} = 1:3, 1:5, 1:9, 1:15,
138 respectively) were tested for Cr(VI) detoxification.

139 2.3. Batch experiments of Cr(VI) removal

140 The influences of initial pH, initial Cr(VI) concentration and different FeS/Fe^0 ratios were
141 studied by batch removal experiments. All the Cr(VI) removal experiments were conducted in
142 three-neck flasks under nitrogen atmosphere. Unless otherwise stated, 0.1 g of the FeS@Fe^0
143 hybrid particles with a Fe^0_{mol}:FeS_{mol} ratio of 9:1 was fed into the three-neck flasks with 200 mL of
144 20 mg/L Cr(VI) solution without pH adjustment (pH ≈ 5.8). The flasks were sealed with rubber
145 screw caps and mechanically stirred during the experiments. The samples were collected by a 2
146 mL syringe at regular time intervals and analyzed immediately after being filtered through a 0.45
147 μm filter membrane. All experiments were conducted at least twice, and the results were averaged.
148 To test the influence of initial pH on removal behavior, the initial pH of Cr(VI) solutions were
149 adjusted by diluted H_2SO_4 and NaOH solutions. To evaluate the Cr(VI) removal efficiency, the
150 data were analyzed by simulating pseudo first-order and pseudo second-order kinetics models.
151 Typical Langmuir model and Freundlich model were used for adsorption isotherms simulation.
152 Supporting information presents the details regarding the equation of these models.

153 Concentrations of aqueous Cr(VI) were measured using a UV-vis spectrometer by the
154 1,5-diphenylcarbazide colorimetric method at wavelength 544 nm. The concentration of total
155 dissolved chromium was analyzed by flame atomic adsorption spectrometry (Flame-AAS, 5100,
156 PerkinElmer, USA). The amount of ferrous ions was spectrophotometrically determined at 510 nm
157 by using the o-phenanthroline method. Total dissolved iron ions were analyzed after reducing ferric
158 ions into ferrous ions by adding hydroxylamine hydrochloride.

159 2.4. Characterization

160 The morphology of the FeS@Fe^0 hybrid particles was studied by field emission scanning
161 electron microscopy (FESEM, Quanta 450 FEG, FEI, USA) coupled to an energy dispersive

spectrometer. The material mineralogy was determined by X-ray diffraction (XRD, X'Pert PRO, PANalytical B.V., the Netherlands). The chemical states of surface elements were recorded by an X-ray photoelectron spectrometer using monochromatic Mg Kα radiation (XPS, VG Multilab 2000, Thermo Electron). To measure the Fourier transform infrared spectra (FTIR), the samples were pressed into tablets with KBr, then analyzed on a Thermo Fisher Nicolet-6700 spectrometer. The BET surface area was measured by N_2 adsorption isotherms at 77 K using an automated surface area and pore size analyzer (ASAP 2020, Micromeritics, USA). Pore volume and pore size distribution plots were obtained by the Barrett-Joyner-Halenda (BJH) method using the cylindrical pore model.

3. Results and discussion

3.1. Characterization of nFe^0 and $FeS@Fe^0$ particles

The morphology and structure of nFe^0 and $FeS@Fe^0$ hybrid particles were characterized by FESEM (Fig. 1). As shown in Fig. 1a, the pristine nFe^0 particles are nanoscale-sized spherical particles and form chain-shaped aggregates. The $FeS@Fe^0$ particles were prepared by coating FeS onto the nFe^0 particles, and found to be a composite, micrometer sized material (Fig. 1b). The irregular small spheres should be the result of nFe^0 particles aggregation, which were then completely covered by amorphous FeS precipitates. The speciation and degree of the crystallinity of nFe^0 and $FeS@Fe^0$ particles were evaluated by XRD characterization. As shown in Fig. 2, nFe^0 shows two sharp 2θ peaks at 44.68 and 65.03°, which correspond to [110] and [200] directions of α-Fe, indicating a high purity and crystallinity of Fe^0. For $FeS@Fe^0$ particles, the XRD pattern of Fe^0 was almost shielded due to the coverage of amorphous FeS. The results obtained from FESEM and XRD characterization indicates that $FeS@Fe^0$ was a hybrid material, and Fe^0 particles were encapsulated by floc-like amorphous FeS.

Specific surface area is an important parameter for adsorption and chemical reduction of Cr(VI). Kim et al. validated that the higher surface area of S-doped nFe^0 was the main reason for its enhanced reactivity towards trichloroethylene (TCE) dechlorination compared to pristine nFe^0 (Kim et al. 2011). The respective BET surface areas of nFe^0 nanoparticles and $FeS@Fe^0$ hybrid particles were measured in terms of N_2 adsorption-desorption isotherms (Fig. S1). Both nFe^0 nanoparticles and $FeS@Fe^0$ hybrid particles exhibited type IV isotherms, indicating the presence of

well-developed mesopores. As summarized in Table 1, nFe^0 has a larger BET surface area, but a smaller pore diameter and pore volume, than $FeS@Fe^0$. This indicated that the enhanced reactivity of $FeS@Fe^0$ cannot be simply ascribed to surface area modification from individual nFe^0.

3.2. Cr(VI) removal kinetics and adsorption isotherm

The kinetics of Cr(VI) removal were investigated over a range of initial Cr(VI) concentration in presence of 0.5 g/L of $FeS@Fe^0$ particles without adjusting the initial pH (pH_0 = 5.0 ~ 5.8). Fig. 3a shows the removal capacity of Cr(VI) as a function of elapsed time. In most cases, the reactions displayed a rapid initial removal rate followed by an equilibrium tail. No more detectable removal of Cr(VI) was achieved after 10 or 30 min of reaction with the initial Cr(VI) concentrations of 10 and 20 mg/L, respectively. The adsorption capacity of $FeS@Fe^0$ reached 57.5 mg/g and 63.9 mg/g with initial Cr(VI) concentrations of 30 and 80 mg/L, indicating an adsorptive saturation at high aqueous Cr(VI) concentration. Increased Cr(VI) concentration would promote the generation of Fe-Cr precipitates, accelerate adsorbent passivation, further limit contaminants diffusion, and block the electron transfer from the Fe^0 core (Lu et al. 2012).

According to the literature, the removal of Cr(VI) using Fe^0-based materials was a multi-step process, involving electrostatic adsorption as well as subsequent Cr(VI) reduction to Cr(III) (Fu et al. 2015, Zhou et al. 2014). To describe the Cr(VI) removal route by $FeS@Fe^0$, pseudo first- and second-order models were used to fit the reaction. As summarized in Table S1, the pseudo first-order model seemed to be unsuitable in describing the Cr(VI) removal because of the low correlation coefficients of the simulations and data, while the pseudo second-order adsorption model performed much better with high correlation coefficients ($R^2 > 0.99$). This simulation result is consistent with many previous reports for Cr(VI) removal by Fe^0-based materials (Ai et al. 2008, Lv et al. 2011, Jiang et al. 2014), implying that chemisorption was the rate-limited process for Cr(VI) removal. Three main steps could occur during Cr(VI) removal: (i) aqueous Cr(VI) oxyanions diffuse to the water-$FeS@Fe^0$ interface, which could be driven via valence forces between surface iron ions and Cr(VI) oxyanions; (ii) Cr(VI) was chemi-adsorbed onto the solid-liquid interface; (iii) Cr(VI) was synchronously reduced to Cr(III). In addition, the reaction rate constants (k_2) of pseudo second-order kinetics decreased with increasing initial Cr(VI)

concentration (Table S1), reconfirming the dependence of the reaction rate on the initial Cr(VI) concentration. Two popular adsorption isotherm models, Langmuir and Freundlich, were used to describe the Cr(VI) adsorption behavior. Fig. 3b shows that the Cr(VI) removal process can be well-described by the Langmuir model with correlation coefficient R^2 values of 0.999. In contrast, the Freundlich model was not suitable to fit the experimental data (Fig. S2). As the Langmuir isotherm was applied to describe monomolecular layer adsorption, therefore, the adsorption of Cr(VI) by FeS@Fe^0 particles occurred mainly homogeneously on the surface via monolayer sorption (Baret 1968, Gupta and Babu 2009). The calculated Q_{max} value, which represent the adsorption capacity of the adsorbent, was 66.7 mg/g. Compared with other Fe-based materials as listed in Table 2, FeS@Fe^0 demonstrated a good ability for Cr(VI) removal.

3.3. Effect of FeS-to-Fe^0 molar ratio on removal of Cr(VI)

The combination of different components resulted in a unique material with new properties. For instance, in previous studies, different doping amounts of dithionite significantly influenced the reactivity of S-doped nFe^0 on TCE or cadmium removal (Kim et al. 2011, Su et al. 2015). Therefore, it is of significance to investigate the reactivity of the FeS@Fe^0 particles with various FeS-to-Fe^0 molar ratios. As shown in Fig. 4, the Cr(VI) removal by FeS@Fe^0 particles with various FeS-to-Fe^0 molar ratios was studied with different adsorbent doses. FeS@Fe^0 particles performed more efficiently on Cr(VI) sequestration than nFe^0, and increasing the adsorbent dose greatly accelerated Cr(VI) removal. Almost all reactions exhibited a good conformity with pseudo-second-order kinetics with high correlation coefficients ($R^2 > 0.99$). Insets of Fig. 4 shows the relationship between the apparent rate constants (k_{obs}) of Cr(VI) removal and the FeS-to-Fe^0 molar ratio. Obviously, the results indicated that the presence of FeS dramatically speeded up the Cr(VI) reduction compared to bare nFe^0. Meanwhile, different molar ratios between FeS and Fe^0 greatly influenced the performances of FeS@Fe^0 particles. The highest k_2 values, irrespective of different FeS@Fe^0 dosages, occurred when the molar ratio of FeS-to-Fe^0 was 1/9, suggesting the fastest Cr(VI) reduction rate. Otherwise, the reaction rate first increased with higher FeS content from 1/15 to 1/9, and then decreased when the FeS content further increased to 1/5 and 1/3. Our results revealed a double-sided effect of post-introduced iron sulfide. As an aqueous electron

acceptor, Cr(VI) can be reduced by direct electron supply from FeS@Fe^0, FeS and generated ferrous ions. Overall, the transfer of electrons from FeS@Fe^0 to the adsorbed Cr(VI) was the rate-limited step. As reported by Mu et al., the mechanism of the anoxic Cr(VI) removal by Fe@Fe_2O_3 nanowires involved electron transfer among various phases (Mu et al. 2014). The proper water aging of the Fe^0 core can generate more surface bound ferrous ions by injecting electrons to the Fe_2O_3 shell due to their different work function. In the present study, FeS was introduced as the shell or cover of the Fe^0 core. Due to the higher electronegativity of FeS (5.02 eV) (Xu and Schoonen 2000) than that of Fe^0 (4.04 eV) (Pearson 1988), electrons generated by Fe^0 corrosion could spontaneously transfer to the FeS semiconductor. Moreover, FeS has a good electron conductivity because of its lower band gap (E_g = 0.1 eV) and a strong reductivity, therefore, facilitating the Cr(VI) reduction via electron acceptance. However, with increasing FeS-to-Fe^0 ratio, too much FeS coverage hindered the reductive removal of Cr(VI). This may be explained by a decreased number of electrons donated from the iron core, the extension of the electron channel length in the FeS semiconductor, and also the oxidation of frontier FeS. Moreover, a large amount of FeS would also inhibit the electrostatic adsorption of Cr(VI) oxyanions because the pH of zero point charges (pH_{PZC}) of FeS is as low as 3.0 (Xu and Schoonen 2000).

3.4. Effect of pH and dissolved oxygen

The solution pH is an important control variable for adsorption and reduction of Cr(VI). Figure 5a shows performance of Cr(VI) uptake by FeS@Fe^0 particles at various initial pHs in the range of 3.0~11.0. Overall, the removal rate of Cr(VI) increases with decreasing pH, similar as previously described in different nFe^0 systems (Hoch et al. 2008, Lv et al. 2014, Li et al. 2012, Fuller et al. 2013). Complete removal of Cr(VI) can be achieved under acidic conditions. The lowest removal efficiency was obtained at the initial pH of 11, wherein 90% of Cr(VI) was removed in 60 min reaction. However, under alkaline conditions, the free and surface bound ferrous ions are more easily oxidized, forming thick hydroxide layers on the surface and further inhibiting Fe^0 corrosion (Zhou et al. 2014). In addition, the FeS@Fe^0 particles would be negatively charged in alkaline solution, hindering the Cr(VI) adsorption due to electrostatic

repulsion. The pH changes before and after the reactions were monitored to reveal the pH effect (Fig. S3). Irrespective of initial pH values, the solution pH moved upward during reactions in most cases except for pH 11, and the final pH values were found in range of 8.5~11.0. For instance, the pH increased to 8.7 after 60 min reaction while the initial pH was 3. The phenomenon of pH rise indicates that the hydronium ion (H^+) is essential and promotional for Cr(VI) reduction (Fuller et al. 2013, Buerge and Hug 1997). As $HCrO_4^-/CrO_4^{2-}$ are predominant species of Cr(VI) at pH < 6, the possible reduction mechanism could be explained by Eq 7~8. Meanwhile, the alkaline conditions after Cr(VI) reduction will be conductive to the adsorptive removal of Cr species due to co-precipitation of Fe(III)/Cr(III) hydroxide.

$$3Fe^{2+} + HCrO_4^- + 7H^+ \rightarrow 3Fe^{3+} + Cr^{3+} + 4H_2O \quad (7)$$

$$Fe^0 + CrO_4^{2-} + 4H_2O \rightarrow Fe(OH)_3 + Cr(OH)_3 + 2OH^- \quad (8)$$

Dissolved oxygen is typically present in surface water and shallow groundwater. To investigate the impact of dissolved oxygen, experiments was conducted by continuously purging vessels with air instead of nitrogen. Figure 5b shows the time profile of Cr(VI) sequestration by FeS@Fe^0 particles under oxic and anoxic conditions, respectively. The presence of oxygen significantly depressed the Cr(VI) removal. The reaction rate under anoxic conditions (k_{anoxic} = 0.023 min^{-1}) exceeds that under oxic conditions (k_{oxic} = 0.0069 min^{-1}) by more than an order of magnitude. Interaction between O_2 and Fe^0 would accelerate iron corrosion and electron transfer from the Fe^0 core (Yoon et al. 2011). However, this positive effect might be negligible since oxygen would compete directly with Cr(VI) to consume surface electrons and Fe(II) species as explained in Eq 9 (Mu et al. 2015).

$$4Fe(II) + O_2 + 10H_2O \rightarrow 4Fe(OH)_3 + 8H^+ \quad (9)$$

The dissolved oxygen could react with surface Fe(II) and generate protons. The pH variation during reactions provides indirect evidence for this phenomenon (Fig. 5b). Under anoxic conditions, the pH rapidly rose in the first 20 min and then reached equilibrium. Nevertheless, a different pathway exists under oxic conditions insofar as the solution pH increased during the initial 20 min as under anoxic conditions, but then dropped for the rest of the reaction time.

The stability of FeS@Fe^0 was further studied by reaction with dissolved oxygen under air purging before using it for Cr(VI) removal. The FeS@Fe^0 material was first mixed and stirred in

water for 30 min with air purging, and then separated by magnet and reused for Cr(VI) removal. As shown in Fig. S4, the reactivity of FeS@Fe^0 decreased after reacting with dissolved oxygen. But this negative impact was limited since 95% of Cr(VI) was removed by used FeS@Fe^0 particles after 60 min reaction, which is still much higher than that obtained by bare nFe^0.

3.8. Mechanism for Cr(VI) removal by FeS@Fe^0 particles

(a) Solid phase analysis

FESEM, XRD, FT-IR and XPS characterizations were further evaluated to understand the change of the speciation, morphology and surface valence state of FeS@Fe^0 particles before and after reactions. FESEM images indicate the morphology transformation of FeS@Fe^0 particles after 60 min of Cr(VI) treatment (Fig. S5a). Cr-treated FeS@Fe^0 particles were aggregated with severe oxidation. The EDX results confirmed the presence of chromium on the surface of Cr-treated nFe^0-FeS particles, which consisted of Cr, S, O and Fe elements (Fig. S5b, Table S2). Chromium partially replaced iron and precipitated in the form of Fe-Cr oxides. Moreover, the atomic ratio of the S element significantly decreased after treatment with Cr(VI), signifying the consumption of sulfides. The XRD spectra of Cr(VI)-treated FeS@Fe^0 particles show that a layer of magnetite formed as a result of iron corrosion compared to fresh particles (Fig. S6), indicating the formation of hydroxychromites-magnetite (Mu et al. 2014, Nahuel Montesinos et al. 2014). The surface functional groups before and after Cr(VI) exposure was determined by FT-IR. As shown in Fig. 6, the FT-IR spectrum of fresh FeS@Fe^0 particles exhibited conspicuous O-H, S-O and S-S vibrations at peaks of 3380 cm^{-1}, 1116 cm^{-1} and 468 cm^{-1}, which were attributed to adsorbed OH, sulfate and sulfide groups, respectively. A slight blue-shift of the O-H stretching peak from 3385 to 3380 cm^{-1} was observed, which could be due to the incorporation of chromium into the hydroxide precipitates. The S-S vibration disappeared and several new peaks at 1051, 1016, and 981 cm^{-1} were found after Cr(VI) treatment, and assigned to S-O vibrations from sulfur compounds. This indicated that iron sulfide was oxidized as FeS was insoluble at pH above 5 throughout the reaction. According to Patterson and Fendorf (Patterson et al. 1997), both sulfide and ferrous are effective for Cr(VI) reduction, and different sulfur phases, including thiosulfate, sulfate and sulfide, were released into solution. Additionally, two Fe-O peak was transformed to

Commented [DW1]: Do you mean the second Fe-O peak?

618 cm^{-1} after Cr adsorption, indicating the formation of Fe-Cr-O precipitates (Rajput et al. 2016).

The valence change of surface elements before and after Cr(VI) treatment was characterized with XPS spectroscopy. In Fig. 7a, the raw Fe 2p spectra of fresh FeS@Fe^0 shows XPS peaks at 710.4 eV and 711.8 eV owing to Fe $2p_{3/2}$ for Fe(II) and Fe(III), respectively (Yamashita and Hayes 2008). Part of Fe(II) species were transformed to Fe(III) after Cr(VI) treatment as identified by spectrum deconvolution. The S 2p XPS spectrum before reaction shows two peaks at 162 eV and 168.6 eV (Fig. 7b), assigned to FeS and surface bound SO_4^{2-} (Du et al. 2016, Toda et al. 2014). After reactions, the S 2p spectrum became three curves positioned at 161 eV, 165 eV, 168 eV, which were corresponding to S^{2-}, SO_3^{2-} or $S_2O_3^{2-}$, and SO_4^{2-} groups, respectively, validating the oxidation of sulfides in presence of Cr(VI). (Zhao et al. 2012, Descostes et al. 2000). The XPS scan of Cr-treated nFe^0-FeS shows a pair of new peaks at 577.0 eV and 586.8 eV (Fig. 7c), validating the transformation of Cr(VI) to Cr(III) in form of $Fe_xCr_{1-x}(OH)_3$ and also $Fe(OH)_3$-$Cr(OH)_3$ as indicated from the O 1s spectra in Fig. 7d (Manning et al. 2008, Nahuel Montesinos et al. 2014). Furthermore, no chromium was detected in aqueous solution after 30 min reaction (Fig. S7), implying that the aqueous Cr(VI) were reduced to Cr(III) and incorporated into FeS@Fe^0 particles. As summarized in Table S3, chromium accounted for 5.4% in terms of atomic ratio, and the ratio of iron and sulfur decreased after treatment with Cr(VI). This is consistent with FT-IR and EDX results. In summary, Cr(VI) was removed by accepting electrons, pairing with oxidation of FeS and Fe^0 as electron donors. The Cr(III) species were destabilized in final alkaline solutions and irreversibly partitioned into the solid phase as Fe-Cr solid precipitates.

(b) Proposed mechanism of Cr(VI) reduction

As stated, Cr(VI) sequestration involved electrostatic adsorption, chemi-reduction and also precipitation processes. The chemisorption in terms of reduction was proposed as the key step during Cr(VI) removal as indicated by kinetic simulation with the pseudo-second-order model and Langmuir isotherm. According to previous studies, Cr(VI) can be reduced by ferrous ions, direct electron donor and even iron sulfide as hypothesized by Eqs 10~12 (Buerge and Hug 1997, Patterson et al. 1997).

$$3Fe(II) + Cr(VI) \rightarrow 3Fe(III) + Cr(III) \quad (10)$$

$$CrO_4^{2-} + 3e^- + 4H_2O \rightarrow Cr^{3+} + 8OH^- \quad (11)$$

$$3CrO_4^{2-} + 2FeS + 9H_2O \rightarrow 4[Cr_{0.75}, Fe_{0.25}](OH)_3 + Fe^{2+} + S_2O_3^{2-} + 6OH^- \quad (12)$$

The role of the generated ferrous ions was investigated by adding 1,10-phenanthroline, which can react as Fe(II) quencher so as to exclude its contribution. Figure 8 shows that the presence of 1,10-phenanthroline significantly inhibited the Cr(VI) reduction. XRD spectra also show that ferrous ions were captured in presence of 1,10-phenanthroline, thus iron oxide was undetected as compared to the fresh sample (Fig. S8). The calculated Cr(VI) removal efficiencies were 100% and 48% for absence versus presence of 1,10-phenanthroline, respectively. This suggests that ferrous ions may contribute 52% to Cr(VI) detoxification. Meanwhile, the phenanthroline-chelated Fe(II) reached as high as 172.8 mg/L in 60 min reaction time, whereas no aqueous Fe(II) was detected during the Cr(VI) reduction in pristine system (Fig. S9). This observation provided strong evidence that ferrous ions were oxidized by Cr(VI) at the solid-solution interface but not in aqueous solution. Surface Fe(II) can be spontaneously regenerated by accepting sustainable electrons from the Fe^0 core. Even though thickened iron oxide shells can be a barrier for electron transfer, the proper thickness of the FeS cover could accelerate electron flow owing to its excellent conductivity and higher electronegativity than Fe^0 particles. However, an overly thick or overly thin FeS layer was unfavorable for Cr(VI) reduction as stated above. As the redox potential of FeS (E^0 = 0.47 V vs. NHE) is lower than that of Cr(VI)/Cr(III) (E^0 =1.35 V vs. NHE) (Bokare and Choi 2011), the direct multi-electron transfer from the conduction band of FeS to sorbed Cr(VI) can spontaneously proceed because such a process is energetically favorable. Then in situ reduction of sorbed Cr(VI) occurred in parallel with oxidation of Fe(II) and FeS, which functioned as electron donors. Iron oxides, such as Fe_3O_4, $Fe(OH)_3$ and FeOOH, and various sulfur compounds were generated as oxidation byproducts. Finally, due to the fast-rising pH, Cr(III) would be highly unstable and irreversibly coprecipitated with iron ions in alkaline conditions to form $Fe_xCr_{1-x}(OH)_3$ and also $Fe(OH)_3$-$Cr(OH)_3$.

Implications for site remediation

Even though nanoscale Fe^0 is one of the most commonly used reactive materials for remediation of Cr(VI) contaminated groundwater and surface water, it exhibited low efficiencies towards Cr(VI) reduction due to iron passivation. The present work validated that the combination

of Fe^0 with FeS can significantly enhance the sequestration and reduction of Cr(VI) oxyanions. Besides, the FeS@Fe^0 hybrid material showed excellent reactivity for rapid removal of Pb(II) and Hg(II) species as shown in Fig. S10. From an economical perspective, the faster treatment and greater removal capacity of the reductive adsorbent will be a significant benefit for site remediation. Compared to the doping with noble metals to form bimetallic Fe^0, such as Pd/Fe, the application of FeS@Fe^0 is much more economic and eco-friendly. Furthermore, this new hybrid material might be assembled in situ when nFe^0 is used for groundwater remediation under sulfur reducing conditions (Jeong et al. 2010), or by immersing the nFe^0 in Na_2S solution before its application. The generated FeS jacket may also reduce the cytotoxicity of Fe^0 particles by separating microorganisms from direct contact with Fe^0 nanoparticles (Kim et al. 2013). Meanwhile, as previously reported, the magnetic property of FeS@Fe^0 particles may also be utilized to facilitate the heavy metals removal and sorbent recovery and regeneration for re-use in wastewater treatment via exerting an outside magnetic field (Huang et al. 2013, Liang et al. 2014). All these advantages make FeS@Fe^0 a promising material for environmental remediation.

Conclusions

In the present study, a magnetic FeS@Fe^0 hybrid material was assembled by wrapping Fe^0 particles with in situ formed amorphous iron monosulfide. The synthesized FeS@Fe^0 has a lower BET surface area but a higher reactivity towards Cr(VI) sequestration than individual nFe^0 particles. The reactivity of FeS@Fe^0 particles varies with the thickness of FeS cover in terms of different FeS-to-Fe^0 molar ratio. The highest Cr(VI) removal efficiency was achieved with the FeS-to-Fe^0 molar ratio of 1/9, and further increasing or decreasing the FeS amount played negative roles. The FeS layer functioned as a conductive channel for electron transmission, which could accelerate the multi-electron transfer from the Fe^0 core to Cr(VI) oxyanions and prevent their rapid passivation by iron oxides. Surface Fe(II), direct electron transfer and reactive sulfide species were validated as the main electron donors for Cr(VI) reduction, which mainly occurred on the solid-liquid interface. Correspondingly, high solution pH and O_2 exposure would significantly inhibited the reduction of Cr(VI). Finally, physical characterization of the fresh and Cr-treated FeS@Fe^0 particles confirmed that Cr(VI) was converted to Cr(III) and completely

immobilized in the solid phase of Fe-Cr hydroxides.

Acknowledgement

This study was funded by National Natural Science Foundation of China (41373083). We thank Dr. Songhu Yuan for his instructive advice. We also thank Xianfan Wang and Wei Kang for their great help for sample analysis.

Appendix A. Supplementary data

References:

Kamaludeen, S.P.B., Megharaj, M., Juhasz, A.L., Sethunathan, N. and Naidu, R. (2003) Chromium-microorganism interactions in soils: remediation implications. Reviews of Environmental Contamination & Toxicology 178, 93-164.

Dhal, B., Thatoi, H.N., Das, N.N. and Pandey, B.D. (2013) Chemical and microbial remediation of hexavalent chromium from contaminated soil and mining/metallurgical solid waste: a review. J Hazard Mater 250-251, 272-291.

Pettine, M., D'Ottone, L., Campanella, L., Millero, F.J. and Passino, R. (1998) The reduction of chromium (VI) by iron (II) in aqueous solutions. Geochimica et Cosmochimica Acta 62(9), 1509-1519.

Cieślak-Golonka, M. (1996) Toxic and mutagenic effects of chromium(VI): A review. Polyhedron 15(21), 3667-3689.

Fu, F., Dionysiou, D.D. and Liu, H. (2014) The use of zero-valent iron for groundwater remediation and wastewater treatment: A review. Journal of Hazardous Materials 267, 194-205.

Du, J., Bao, J., Tong, M. and Yuan, S. (2013) Dechlorination of Pentachlorophenol by Palladium/Iron Nanoparticles Immobilized in a Membrane Synthesized by Sequential and Simultaneous Reduction of Trivalent Iron and Divalent Palladium Ions. Environmental Engineering Science 30(7), 350-356.

Huang, P., Ye, Z., Xie, W., Chen, Q., Li, J., Xu, Z. and Yao, M. (2013) Rapid magnetic removal of aqueous heavy metals and their relevant mechanisms using nanoscale zero valent iron (nZVI) particles. Water Research 47(12), 4050-4058.

Guan, X., Sun, Y., Qin, H., Li, J., Lo, I.M., He, D. and Dong, H. (2015) The limitations of applying zero-valent iron technology in contaminants sequestration and the corresponding countermeasures: the development in zero-valent iron technology in the last two decades (1994-2014). Water Research 75, 224-248.

Manning, B.A., Kiser, J.R., Kwon, H. and Kanel, S.R. (2008) Spectroscopic Investigation of Cr(III)- and Cr(VI)-Treated Nanoscale Zerovalent Iron. Environ. Sci. Technol. 41(2), 586-592.

Ai, Z., Cheng, Y., Zhang, L. and Qiu, J. (2008) Efficient removal of Cr(VI) from aqueous solution with Fe@Fe_2O_3 core-shell nanowires. Environmental Science & Technology 42(18), 6955-6960.

Hoch, L.B., Mack, E.J., Hydutsky, B.W., Hershman, J.M., Skluzacek, J.M. and Mallouk, T.E. (2008) Carbothermal Synthesis of Carbon-supported Nanoscale Zero-valent Iron Particles for the Remediation of Hexavalent Chromium. Environmental Science & Technology 42(7), 2600-2605.

Yoon, I.H., Bang, S., Chang, J.S., Min, G.K. and Kim, K.W. (2011) Effects of pH and dissolved oxygen on

462 Cr(VI) removal in Fe(0)/H_2O systems. Journal of Hazardous Materials 186(1), 855–862.
463 Melitas, N., Chuffe-Moscoso, O. and Farrell, J. (2001) Kinetics of soluble chromium removal from
464 contaminated water by zerovalent iron media: corrosion inhibition and passive oxide effects. Environ.
465 Sci. Technol. 35(35), 3948-3953.
466 Huang, Y.H. and Zhang, T.C. (2005) Effects of dissolved oxygen on formation of corrosion products and
467 concomitant oxygen and nitrate reduction in zero-valent iron systems with or without aqueous Fe 2+.
468 Water Research 39(9), 1751-1760.
469 Kim, E.-J., Kim, J.-H., Azad, A.-M. and Chang, Y.-S. (2011) Facile synthesis and characterization of Fe/FeS
470 nanoparticles for environmental applications. Appl. Mater. Interfaces 3, 1457-1462.
471 Fan, D., Anitori, R.P., Tebo, B.M., Tratnyek, P.G., Lezama Pacheco, J.S., Kukkadapu, R.K., Engelhard,
472 M.H., Bowden, M.E., Kovarik, L. and Arey, B.W. (2013) Reductive Sequestration of Pertechnetate
473 ($99TcO^{4-}$) by Nano Zerovalent Iron (nZVI) Transformed by Abiotic Sulfide. Environmental Science &
474 Technology 47(10), 5302-5310.
475 Lv, X., Jiang, X., Jiang, G., Jie, T. and Xu, X. (2011) Highly active nanoscale zero-valent iron (nZVI)–Fe_3O_4
476 nanocomposites for the removal of chromium(VI) from aqueous solutions. Journal of Colloid &
477 Interface Science 369(1), 460-469.
478 Mu, Y., Ai, Z., Zhang, L. and Song, F. (2014) Insight into core–shell dependent anoxic Cr(VI) removal
479 with Fe@Fe_2O_3 nanowires: Indispensable role of surface bound Fe(II). Acs Applied Materials &
480 Interfaces 7(3).
481 Lv, X., Xue, X., Jiang, G., Wu, D., Sheng, T., Zhou, H. and Xu, X. (2014) Nanoscale zero-valent iron (nZVI)
482 assembled on magnetic Fe_3O_4/graphene for chromium (VI) removal from aqueous solution. Journal of
483 Colloid & Interface Science 417(3), 51–59.
484 Gong, Y., Liu, Y., Xiong, Z. and Zhao, D. (2014) Immobilization of mercury by carboxymethyl cellulose
485 stabilized Iron sulfide nanoparticles: Reaction mechanisms and effects of stabilizer and water
486 chemistry. Environmental Science & Technology 48(7), 3986-3994.
487 Bi, Y. and Hayes, K.F. (2014) Nano-FeS Inhibits UO_2 Reoxidation under Varied Oxic Conditions.
488 Environmental Science & Technology 48(1), 632-640.
489 Jeong, H.Y. and Hayes, K.F. (2007) Reductive Dechlorination of Tetrachloroethylene and
490 Trichloroethylene by Mackinawite (FeS) in the Presence of Metals: Reaction Rates. Environmental
491 Science & Technology 41(18), 6390-6396.
492 Kim, E.-J., Kim, J.-H., Chang, Y.-S., Turcio-Ortega, D. and Tratnyek, P.G. (2014) Effects of Metal Ions on
493 the Reactivity and Corrosion Electrochemistry of Fe/FeS Nanoparticles. Environmental Science &
494 Technology 48(7), 4002-4011.
495 Su, Y., Adeleye, A.S., Keller, A.A., Huang, Y., Dai, C., Zhou, X. and Zhang, Y. (2015) Magnetic
496 sulfide-modified nanoscale zerovalent iron (S-nZVI) for dissolved metal ion removal. Water Research
497 74, 47-57.
498 Lu, X., Li, M., Tang, C., Feng, C. and Liu, X. (2012) Electrochemical depassivation for recovering Fe^0
499 reactivity by Cr(VI) removal with a permeable reactive barrier system. Journal of Hazardous Materials
500 213–214, 355-360.
501 Fu, R., Yang, Y., Xu, Z., Zhang, X., Guo, X. and Bi, D. (2015) The removal of chromium (VI) and lead (II)
502 from groundwater using sepiolite-supported nanoscale zero-valent iron (S-NZVI). Chemosphere 138,
503 726-734.
504 Zhou, S., Li, Y., Chen, J., Liu, Z., Wang, Z. and Na, P. (2014) Enhanced Cr(VI) removal from aqueous
505 solutions using Ni/Fe bimetallic nanoparticles: characterization, kinetics and mechanism. RSC

506 Advances 4(92), 50699-50707.
507 Jiang, W., Cai, Q., Xu, W., Yang, M., Cai, Y., Dionysiou, D.D. and O'Shea, K.E. (2014) Cr(VI) Adsorption
508 and Reduction by Humic Acid Coated on Magnetite. Environmental Science & Technology 48(14),
509 8078-8085.
510 Baret, J.F. (1968) Kinetics of adsorption from a solution. Role of the diffusion and of the
511 adsorption-desorption antagonism. The Journal of Physical Chemistry 72(8), 2755-2758.
512 Gupta, S. and Babu, B.V. (2009) Removal of toxic metal Cr(VI) from aqueous solutions using sawdust as
513 adsorbent: Equilibrium, kinetics and regeneration studies. Chemical Engineering Journal 150(2–3),
514 352-365.
515 Xu, Y. and Schoonen, M.A.A. (2000) The absolute energy positions of conduction and valence bands of
516 selected semiconducting minerals. American Mineralogist 85(3-4), 543-556.
517 Pearson, R.G. (1988) Absolute electronegativity and hardness: application to inorganic chemistry.
518 Inorganic Chemistry 27(4), 734-740.
519 Li, Y., Li, J. and Zhang, Y. (2012) Mechanism insights into enhanced Cr(VI) removal using nanoscale
520 zerovalent iron supported on the pillared bentonite by macroscopic and spectroscopic studies. Journal
521 of Hazardous Materials 227–228, 211-218.
522 Fuller, S.J., Stewart, D.I. and Burke, I.T. (2013) Chromate Reduction in Highly Alkaline Groundwater by
523 Zerovalent Iron: Implications for Its Use in a Permeable Reactive Barrier. Industrial & Engineering
524 Chemistry Research 52(13), 4704-4714.
525 Buerge, I.J. and Hug, S.J. (1997) Kinetics and pH Dependence of Chromium(VI) Reduction by Iron(II).
526 Environmental Science & Technology 31(5), 1426-1432.
527 Mu, Y., Wu, H. and Ai, Z. (2015) Negative impact of oxygen molecular activation on Cr(VI) removal with
528 core–shell Fe@Fe_2O_3 nanowires. Journal of Hazardous Materials 298, 1-10.
529 Nahuel Montesinos, V., Quici, N., Beatriz Halac, E., Leyva, A.G., Custo, G., Bengio, S., Zampieri, G. and
530 Litter, M.I. (2014) Highly efficient removal of Cr(VI) from water with nanoparticulated zerovalent iron:
531 Understanding the Fe(III)–Cr(III) passive outer layer structure. Chemical Engineering Journal 244,
532 569-575.
533 Patterson, R.R., Fendorf, S. and Fendorf, M. (1997) Reduction of Hexavalent Chromium by Amorphous
534 Iron Sulfide. Environmental Science & Technology 31(7), 2039-2044.
535 Rajput, S., Pittman Jr, C.U. and Mohan, D. (2016) Magnetic magnetite (Fe_3O_4) nanoparticle synthesis
536 and applications for lead (Pb^{2+}) and chromium (Cr^{6+}) removal from water. Journal of Colloid and
537 Interface Science 468, 334-346.
538 Yamashita, T. and Hayes, P. (2008) Analysis of XPS spectra of Fe2+ and Fe3+ ions in oxide materials.
539 Applied Surface Science 254(8), 2441-2449.
540 Du, J., Bao, J., Fu, X., Lu, C. and Kim, S.H. (2016) Mesoporous sulfur-modified iron oxide as an effective
541 Fenton-like catalyst for degradation of bisphenol A. Applied Catalysis B: Environmental 184, 132-141.
542 Toda, K., Tanaka, T., Tsuda, Y., Ban, M., Koveke, E.P., Koinuma, M. and Ohira, S.-I. (2014) Sulfurized
543 limonite as material for fast decomposition of organic compounds by heterogeneous Fenton reaction.
544 Journal of Hazardous Materials 278, 426-432.
545 Zhao, L., Li, X., Hao, C. and Raston, C.L. (2012) SO_2 adsorption and transformation on calcined NiAl
546 hydrotalcite-like compounds surfaces: An in situ FTIR and DFT study. Applied Catalysis B:
547 Environmental 117–118, 339-345.
548 Descostes, M., Mercier, F., Thromat, N., Beaucaire, C. and Gautier-Soyer, M. (2000) Use of XPS in the
549 determination of chemical environment and oxidation state of iron and sulfur samples: constitution of

a data basis in binding energies for Fe and S reference compounds and applications to the evidence of surface species of an oxidized pyrite in a carbonate medium. Applied Surface Science 165(4), 288-302.
Bokare, A.D. and Choi, W. (2011) Advanced oxidation process based on the Cr(III)/Cr(VI) redox cycle. Environ Sci Technol 45(21), 9332-9338.
Jeong, H.Y., Han, Y.-S., Park, S.W. and Hayes, K.F. (2010) Aerobic oxidation of mackinawite (FeS) and its environmental implication for arsenic mobilization. Geochimica et Cosmochimica Acta 74(11), 3182-3198.
Kim, E.-J., Le Thanh, T., Kim, J.-H. and Chang, Y.-S. (2013) Synthesis of metal sulfide-coated iron nanoparticles with enhanced surface reactivity and biocompatibility. RSC Advances 3(16), 5338-5340.
Liang, L., Sun, W., Guan, X., Huang, Y., Choi, W., Bao, H., Li, L. and Jiang, Z. (2014) Weak magnetic field significantly enhances selenite removal kinetics by zero valent iron. Water Research 49, 371-380.
Hu, J., Chen, G. and Lo, I.M.C. (2005) Removal and recovery of Cr(VI) from wastewater by maghemite nanoparticles. Water Research 39(18), 4528-4536.
Huang, S.-H. and Chen, D.-H. (2009) Rapid removal of heavy metal cations and anions from aqueous solutions by an amino-functionalized magnetic nano-adsorbent. Journal of Hazardous Materials 163(1), 174-179.

Figure Captions:

Figure 1. FESEM images of freshly prepared (a) nFe^0 and (b) $FeS@Fe^0$.

Figure 2. XRD patterns of freshly prepared nFe^0 and $FeS@Fe^0$.

Figure 3. (a) Removal kinetics of Cr(VI) by $FeS@Fe^0$ (Symbols stand for the experimental data and dashed lines stand for the pseudo-second-order fitting); (b) Langmuir isotherm of Cr(VI) adsorption. The reactions were carried out at initial Cr(VI) concentrations of 10 to 80 mg/L with 0.5 g/L $FeS@Fe^0$, 293 K and without pH adjusting ($pH_0 \approx 5.8$).

Figure 4. Effect of different FeS-to-Fe^0 molar ratios on Cr(VI) uptake by $FeS@Fe^0$ particles with various dosages (inset shows the pseudo-second-order kinetic constants at different FeS-to-Fe^0 molar ratios): (a) $FeS@Fe^0$= 0.5 g/L, (b) $FeS@Fe^0$= 1.0 g/L, (c) $FeS@Fe^0$= 1.5 g/L. Conditions: $[Cr(VI)]_0$ = 20 mg/L, N_2 protection, 293 K and without pH adjusting ($pH_0 \approx 5.8$).

Figure 5. Effect of (a) initial pH; (b) comparison of Cr(VI) removal by $FeS@Fe^0$ particles under anoxic and oxic conditions.

Figure 6. FTIR spectra of fresh $FeS@Fe^0$ and collected $FeS@Fe^0$ particles after reacting with 20 mg/L of Cr(VI) under anoxic conditions.

Figure 7. XPS spectra of (a) the Fe 2p region, (b) the S 2p region, (c) the O 1s region and (d) the Cr 2p region of the fresh and Cr-loaded $FeS@Fe^0$ sample.

Figure 8. Removal efficiency of Cr(VI) by $FeS@Fe^0$ in absence or presence of 1,10-phenanthroline or EDTA. Concentrations: [$FeS@Fe^0$] = 0.5 g/L, [Cr(VI)] = 20 mg/L, [1,10-phenanthroline] = 5.0 mmol/L if added, [EDTA] = 5.0 mmol/L if added.

Scheme 1. Proposed working mechanism for Cr(VI) removal by $FeS@Fe^0$ particles

Table Captions:

Table 1. BET surface area and pore volume parameters for nFe^0 and nFe^0-FeS.

Table 2. Adsorption capacities of various Fe-based adsorbents for Cr(VI) removal.

595 **Figure 1**

596 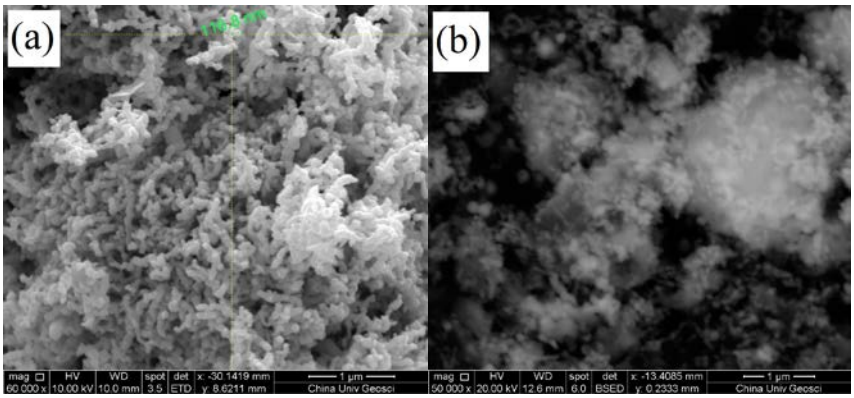

597

598

Figure 2

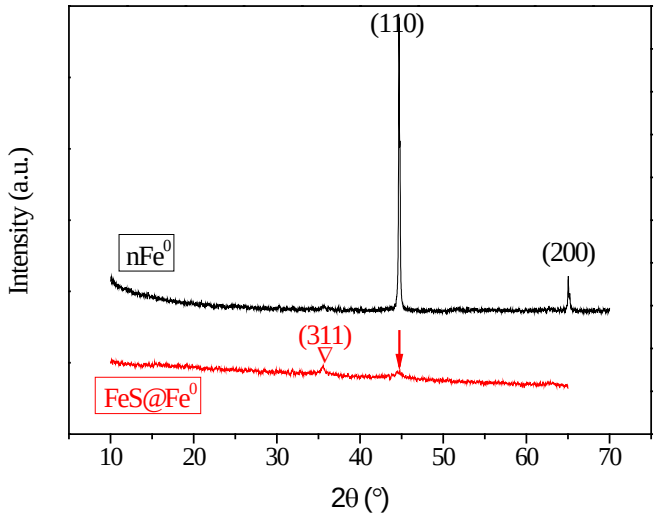

602 **Figure 3**

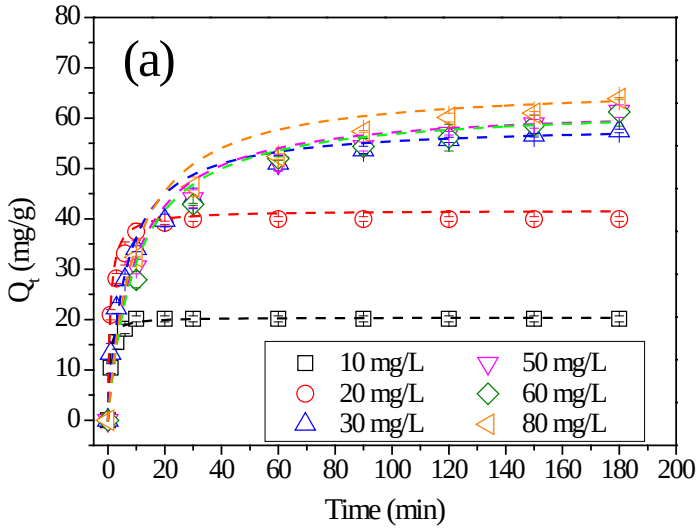

603

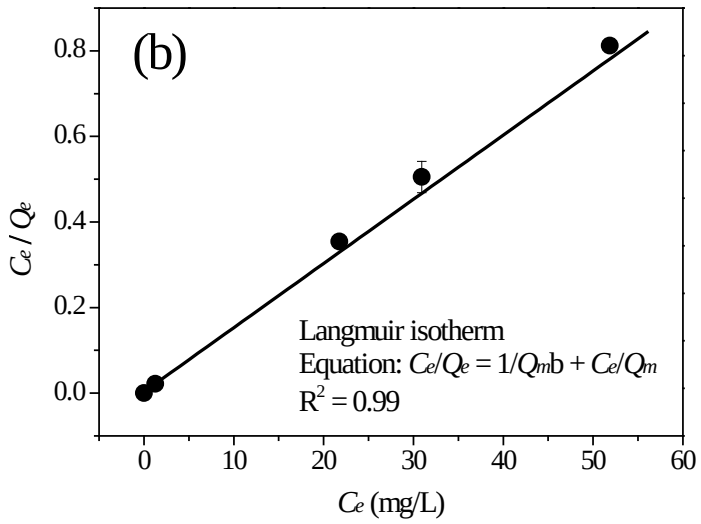

604

605

606 **Figure 4**

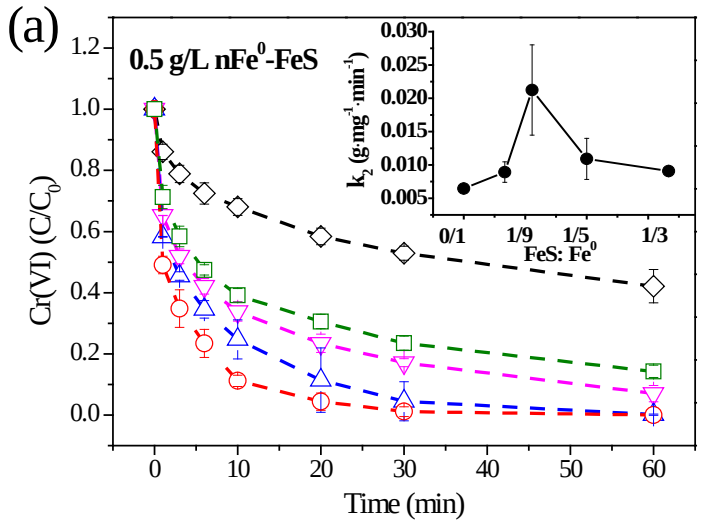

607

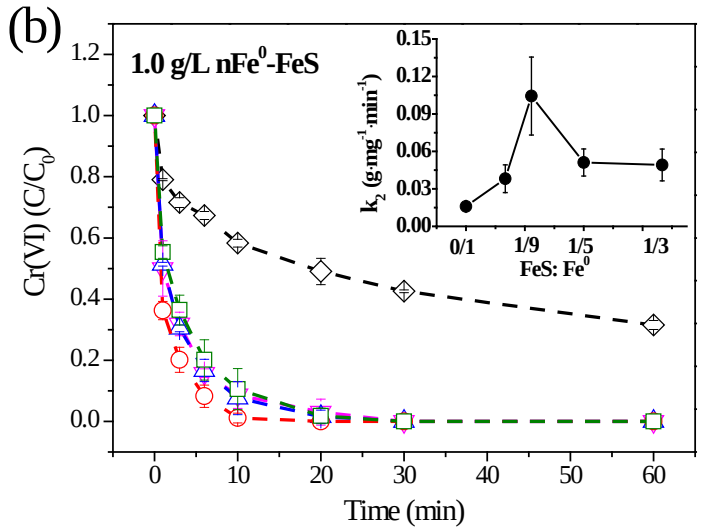

608

609

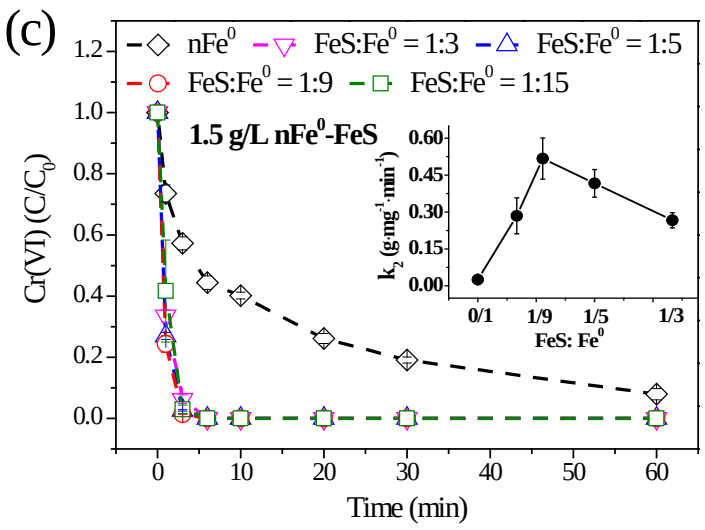
(c)
nFe0
FeS:Fe0 = 1:3
FeS:Fe0 = 1:5
FeS:Fe0 = 1:9
FeS:Fe0 = 1:15
1.5 g/L nFe0-FeS
Cr(VI) (C/C0)
Time (min)
k2 (g·mg-1·min-1)
FeS: Fe0
0/1
1/9
1/5
1/3

610

611 **Figure 5**

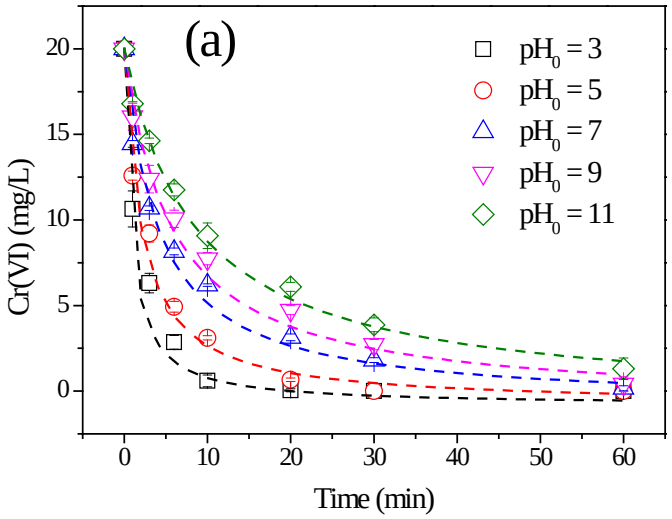

612

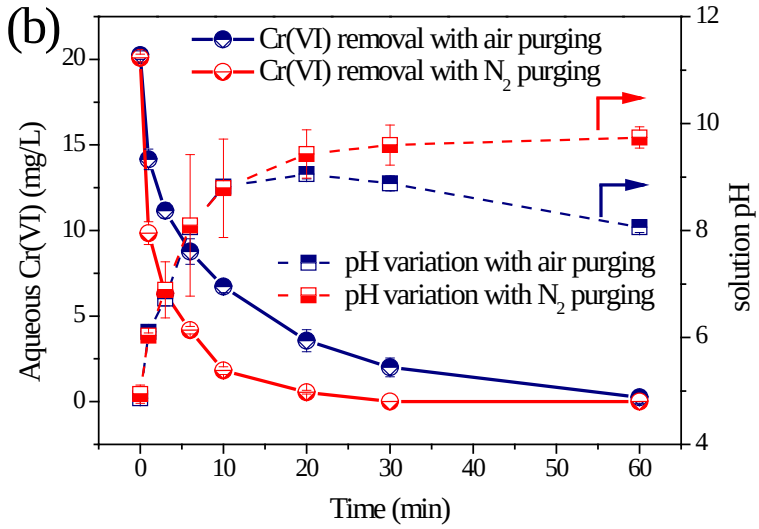

613

614 **Figure 6**

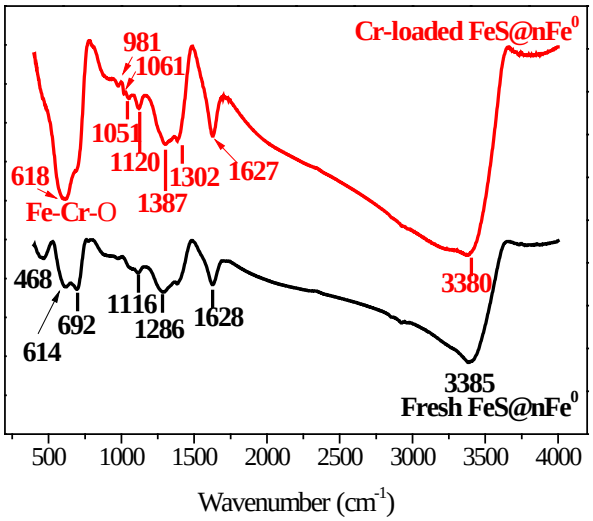

615
616

617 **Figure 7**

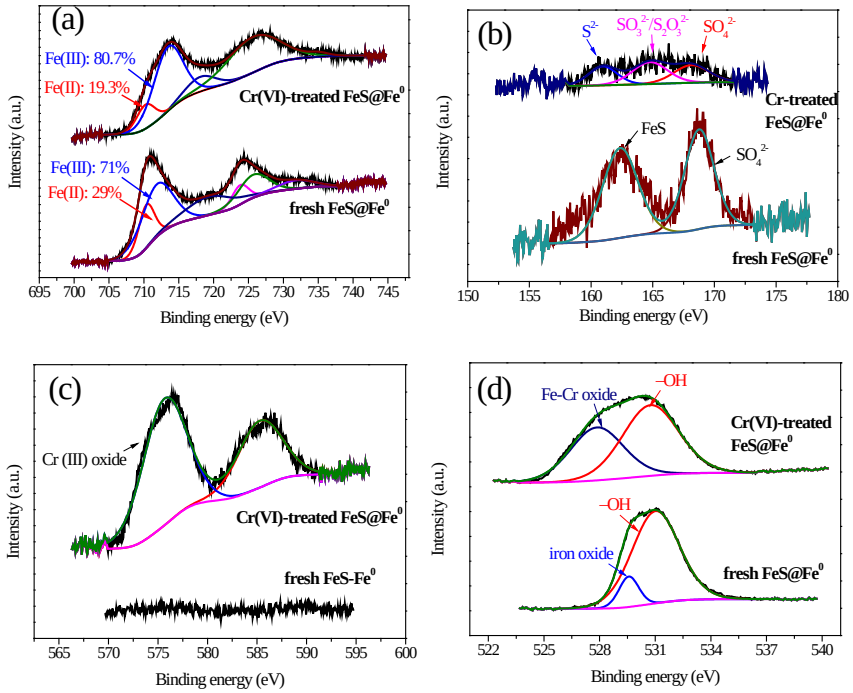

618

619

620

621 **Figure 8**

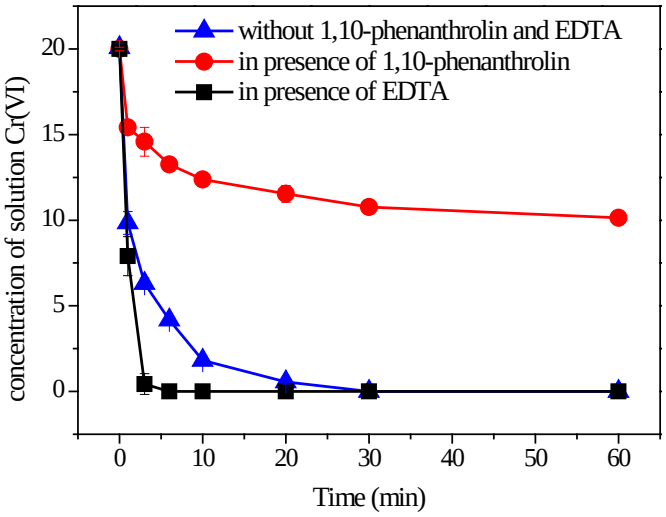

622
623

624

625 **Scheme 1**

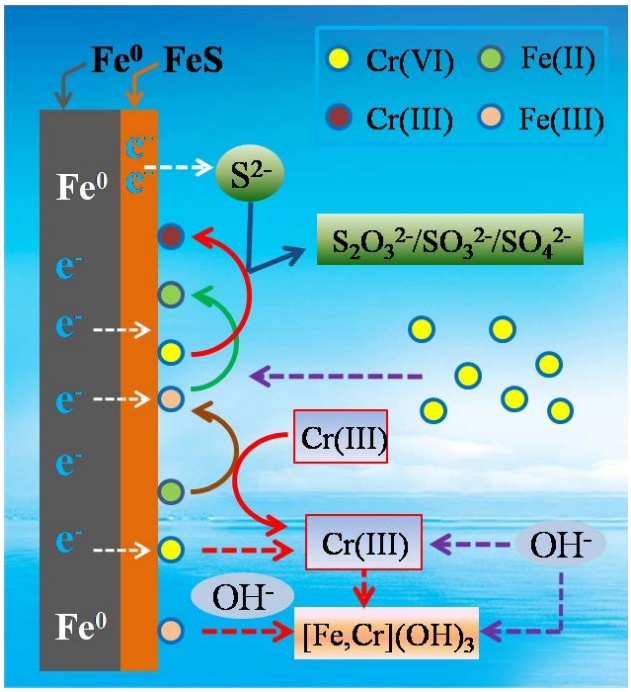

626

627

628 **Table 1**

sample	S_{BET} [a] (m^2/g)	D_{ads} [b] (nm)	V_{ads} [c] (cm^3/g)
nFe^0	77.66	8.76	0.074
$FeS@Fe^0$	53.11	27.84	0.170

629 Note: [a] S_{BET}: BET surface area; [b] D_{ads}: BJH adsorption average pore diameter; [c] V_{ads}: BJH
630 adsorption cumulative pore volume of pores

631

632

633 **Table 2**

sample	pH	Adsorption capacity ($mg \cdot g^{-1}$)	Reference
nZVI-Fe_3O_4	8.0	29.4	(Lv et al. 2011)
nZVI-Fe_3O_4	3.0	100.0	(Lv et al. 2011)
Fe_3O_4 NPs	2.0	19.2	(Hu et al. 2005)
Amino-modified Fe_3O_4 NPs	2.0	11.2	(Huang and Chen 2009)
Nano Fe^0	3.0	17.61	(Zhou et al. 2014)
Nano Ni/Fe^0	3.0	22.59	(Zhou et al. 2014)
sepiolite-supported nZVI	4.0	43.86	(Fu et al. 2015)
$FeS@Fe^0$	5.6	66.7	present work

634 Note: nZVI represents nanoscale zero-valent iron; NPs represents nanoparticles.